Interface Focus

Interface Focus (2011) **1**, 665–672
doi:10.1098/rsfs.2011.0018
Published online 1 June 2011

Review

Continuous wave ultrasonic Doppler tomography

Haidong-Dong Liang[1,2,*], Chun Sing Louis Tsui[1], Michael Halliwell[1] and Peter N. T. Wells[2]

[1]*Department of Medical Physics and Bioengineering, University Hospitals Bristol NHS Foundation Trust, Bristol General Hospital, Bristol BS1 6SY, UK*
[2]*School of Engineering, Cardiff University, Queen's Buildings, The Parade, Cardiff CF24 3AA, UK*

In continuous wave ultrasonic Doppler tomography (DT), the ultrasonic beam moves relative to the scanned object to acquire Doppler-shifted frequency spectra which correspond to cross-range projections of the scattering and reflecting structures within the object. The relative motion can be circular or linear. These data are then backprojected to reconstruct the two-dimensional image of the object cross section. By using coherent processing, the spatial resolution of ultrasonic DT is close to an order of magnitude better than that of traditional pulse-echo imaging at the same ultrasound frequency.

Keywords: Doppler tomography; ultrasonic imaging; medical imaging; coherent processing; incoherent processing

1. INTRODUCTION

Contemporary biomedical ultrasonic imaging is usually based on the pulse-echo method [1]. The principle is that the distance along an ultrasonic beam between a transducer and a reflective target can be calculated from the time delay between the transmission of an ultrasonic pulse and the reception of its echo, assuming that the propagation speed in the intervening medium is known. If the distance between two targets is less than the pulse length, they cannot be discriminated; therefore, the shorter the pulse, the better the spatial resolution. The wavelength of the ultrasound (US; about 1 mm in water and tissue at a frequency of 1.5 MHz, and proportionately less at higher frequencies) fundamentally determines the spatial resolution. Because the attenuation of US in tissue increases with the ultrasonic frequency, however, the improvement in the spatial resolution at any given penetration which can be obtained simply by increasing the frequency is limited by noise. The contrast resolution depends on differences in the reflectivities or scattering powers of the tissues and on the dynamic range of the imaging system. Considering the pulse-echo principle, it is natural to think that continuous wave (CW) US is not suitable for imaging owing to its long (or its, effectively, infinitely long) pulse duration [2]. Thus, the Doppler phenomenon associated with CW has generally been limited to the detection of movement of tissue, such as blood flow [3].

However, it is possible to apply CW to generate US images using a special case of the Doppler phenomenon that is caused by relative movement between the target and the probe. This US imaging modality is termed the 'Doppler tomography' (DT) method [4]; it should not be confused with another class of tomography method called ultrasonic computed tomography (UCT) [5,6], which uses pulse (transmission mode) or pulse-echo (reflection mode) US.

In ultrasonic DT, the tissue to be imaged is moved with respect to an ultrasonic beam and reflecting and scattering targets within the tissue return echoes that are correspondingly Doppler-shifted in frequency. A tomographic method has been used to detect the existence of flowing fluid in a phantom (a physical model simulating relevant anatomical features); however, neither the phantom nor the transducer was moved to cause the Doppler effect and, therefore, only the fluid flow was detected [7]. Ultrasonic imaging using the Doppler effect caused by a linearly moving transducer has also been demonstrated [8]. The idea of rotating the targets to cause the ultrasonic Doppler effect for spatial imaging was first proposed more than 30 years ago [9], but was not realized until we constructed a system for incoherent CW ultrasonic DT [4,10–12]. Thus, this is different from the established method of Doppler imaging in which the Doppler effect is caused by physiological movement of the blood or tissues.

*Author for correspondence (haidong.liang@hotmail.co.uk).

One contribution of 15 to a Theme Issue 'Recent advances in biomedical ultrasonic imaging techniques'.

Received 28 February 2011
Accepted 9 May 2011

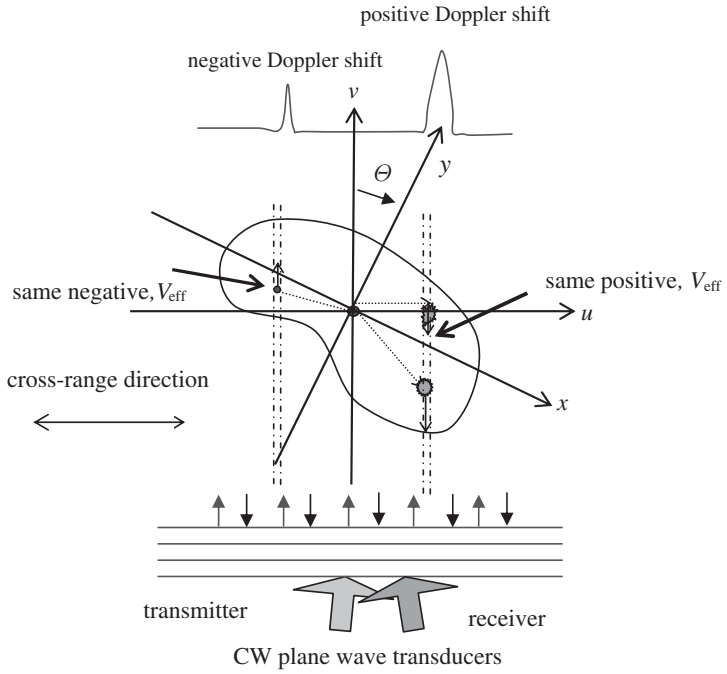

Figure 1. Geometry of circular Doppler tomography.

This review describes the principles of CW ultrasonic DT imaging and presents some experimental results.

2. CIRCULAR MOTION DOPPLER TOMOGRAPHY

2.1. Basic principles

The phenomenon of the Doppler effect caused by a rotating object was first used in radar or microwave imaging [13–17]. Considering the scanning geometry illustrated in figure 1, when an object rotates within the CW beam of a stationary ultrasonic transducer, the scattering centres within the object return echoes that are Doppler-shifted in frequency by amounts depending on the velocities of the individual scatterers. At any given instant, the scatterers that lie on a line of constant cross-range (i.e. the length of the perpendicular from the ray passing through the centre of rotation to the scatterers) all have the same effective velocity in the direction pointing towards to the transducer. Having the same velocity, the scatterers that lie on a line of constant cross-range all reradiate the same Doppler-shifted frequency towards the receiving transducer. The amplitude of the received signal at that frequency yields the line integral of the scattered radiation at that cross-range. By extracting the amplitudes of all the frequencies, the line integrals are obtained for all the scatterers at their corresponding cross-ranges. The ensemble of integral data can be interpreted as a projection. While the object continuously rotates to a new angle, another projection is measured. It is clear that projections obtained by the Doppler effect caused by a rotating object resemble those used in X-ray computed tomography (CT), in which projections are obtained by passing a set of narrow X-ray beams through the object and detecting their intensities using an array of sensors positioned at the opposite side [18].

2.2. Incoherent processing

In practice, it is required that the data obtained with one half-revolution of the object are divided into a number of windows (with or without overlap) and the frequency spectrum of each window is used as the line projection data, as required for backprojection. In other words, the number of data points in the frequency spectrum (i.e. the window length) defines the number of rays (in CT terms).

For each projection, if only the amplitude of the frequency spectrum is used, the method is considered to be incoherent processing [19]. Assuming identical resolution in radial and circumferential directions, the spatial resolution Δ can be derived [4],

$$\Delta = \sqrt{\frac{R\lambda}{2}}, \tag{2.1}$$

where R is the object size and λ is the wavelength.

A spatial resolution of about four wavelengths was achieved with incoherent imaging on an object with diameter of 8 mm using 10 MHz US [4]. The resolution is determined by the compromise between the frequency resolution and the rotation speed. Although increasing the rotation speed increases the Doppler frequency shift (leading to better radial resolution), the information gathered is in a wider angle and this decreases the circumferential resolution.

2.3. Coherent processing

In contrast to the incoherent processing method described above, higher spatial resolution can be achieved by incorporating inphase/quadrature (I/Q) sampling data acquisition and using coherent processing [19,20].

Consider the two-dimensional geometry with global coordinates on the (u, v) plane, as illustrated in figure 1, where an object with local coordinates on the (x, y)

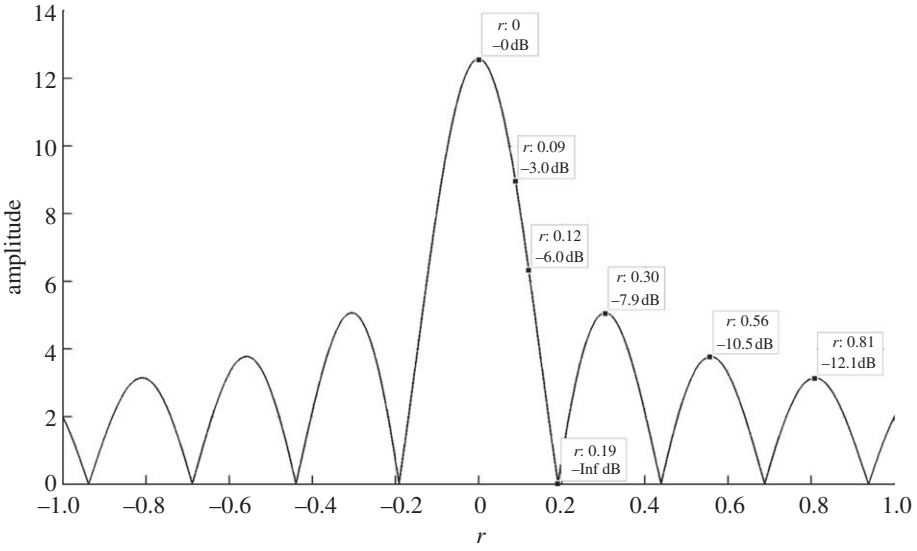

Figure 2. The PSF of coherent Doppler tomography. The unit of the x-axis is λ (wavelength) and that of y-axis is relative.

plane is rotating around an axis orthogonal to the plane with uniform angular velocity centred at (0, 0). A probe is located at a distance away from the centre of rotation and uniformly insonates the object with CW US. Here, we assume that the US beam is infinitesimally thin; therefore, out-of-plane reflections are ignored. In practice, it is an integral along the z-axis. The centre of the rotation does not translate or move during acquisition. With $g(x, y)$ representing the reflectivity function of the object, as Doppler-shifted data are acquired continuously for one cycle of rotation from different object aspect angles $\boldsymbol{\Theta}$, the received I/Q signal $S(\boldsymbol{\Theta})$ can be expressed as a continuous function of the target reflectivity [20,21],

$$S(\boldsymbol{\Theta}) = \int_{-\infty}^{\infty}\int_{-\infty}^{\infty} g(x, y)\exp \times \left[-j\frac{4\boldsymbol{\pi}}{\boldsymbol{\lambda}}(-x\sin\boldsymbol{\Theta} + y\cos\boldsymbol{\Theta})\right]\mathrm{d}x\,\mathrm{d}y, \quad (2.2)$$

where $\boldsymbol{\Theta} = \boldsymbol{\omega}t$ and $\boldsymbol{\omega}$ is the angular velocity. If we let

$$\left.\begin{aligned} f_x &= \left(\frac{2}{\boldsymbol{\lambda}}\right)\sin\boldsymbol{\Theta} \\ \text{and} \qquad f_y &= \left(-\frac{2}{\boldsymbol{\lambda}}\right)\cos\boldsymbol{\Theta}, \end{aligned}\right\} \quad (2.3)$$

equation (2.2) can be rewritten as

$$S(f_x,\ f_y) = \int_{-\infty}^{\infty}\int_{-\infty}^{\infty} g(x, y)\exp[j2\boldsymbol{\pi}(f_x x + f_y y)]\,\mathrm{d}x\,\mathrm{d}y. \quad (2.4)$$

It can be seen that $S(f_x, f_y)$ is the two-dimensional Fourier transform of $g(x, y)$, Therefore, the inverse Fourier transform of $S(f_x, f_y)$ gives the predicted image $\hat{g}(x, y)$on a Cartesian raster,

$$\hat{g}(x, y) = \int_{-\infty}^{\infty}\int_{-\infty}^{\infty} S(f_x, f_y)\exp[-j2\boldsymbol{\pi}(f_x x + f_y y)]\mathrm{d}f_x\,\mathrm{d}f_y. \quad (2.5)$$

2.3.1. Spatial resolution. By considering the polar coordinates system $(\boldsymbol{\rho}, \boldsymbol{\Theta})$, the impulse response can be obtained in the spatial domain with polar coordinate (r, θ) [19],

$$h(r, \theta) = \frac{4\boldsymbol{\pi}}{\boldsymbol{\lambda}} J_0\left(\frac{4\boldsymbol{\pi}}{\boldsymbol{\lambda}} r\right), \quad (2.6)$$

where $J_0(\cdot)$ is the zero-order Bessel function of the first kind.

The meaning of the impulse response (i.e. the point-spread function; PSF) $h(r, \theta)$ is that the PSF is the image of an ideal point scatterer with infinitely small size. The PSF exhibits radial symmetry (figures 2 and 3). In this case, it is imaged as a main lobe surrounded by monotonically decreasing circular side lobes. The imaging system is linear and spatially shift-invariant under the assumption that the size of the target is much smaller than its distance from the probe. The form of the response is uniform throughout the object space. The image response to multiple point objects is the superposition of the PSFs, weighted by their amplitudes and shifted to the positions of the individual scatterers.

According to figures 2 and 3, the distance between the peak of the main lobe and the first zero is $0.19\boldsymbol{\lambda}$. The peak of the first side lobe is $0.3\boldsymbol{\lambda}$ away from that of the main lobe. The amplitude is 8 dB below that of the main lobe.

The side lobes can be suppressed if multiple frequencies (or wavelengths) are used. In this approach, the position of the peak of the main lobe remains the same, while the positions of the side lobes change according to the wavelength. The summation of the PSFs at various wavelengths results in lowered side lobes. However, the multiple frequency approach would reduce the frame rate of the imaging. The other approach is to position the transmitter and receiver at different locations so as passively to achieve the change of the carrier frequency [22].

According to the PSF, the full-width half-maximum (FWHM) spatial resolution of circular coherent DT is

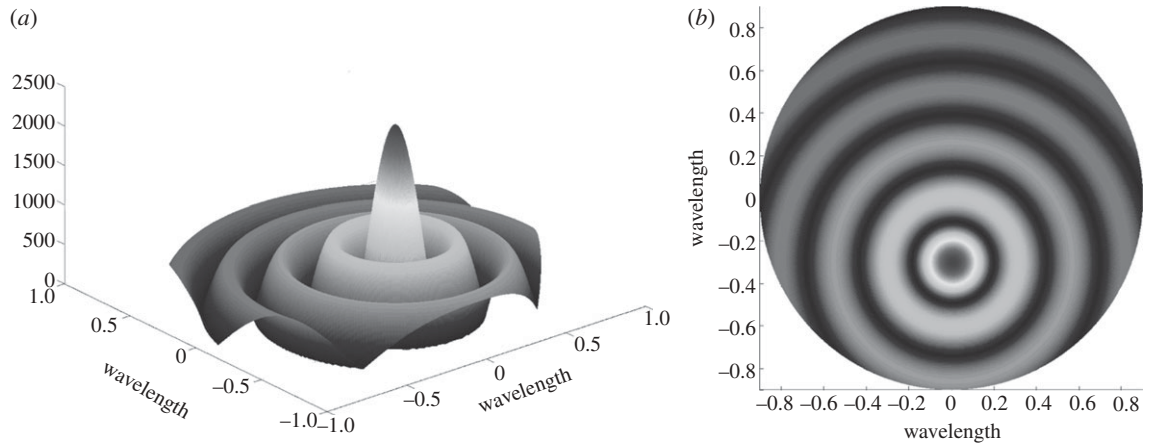

Figure 3. (*a*) Three- and (*b*) two-dimensional views of the point-spread function.

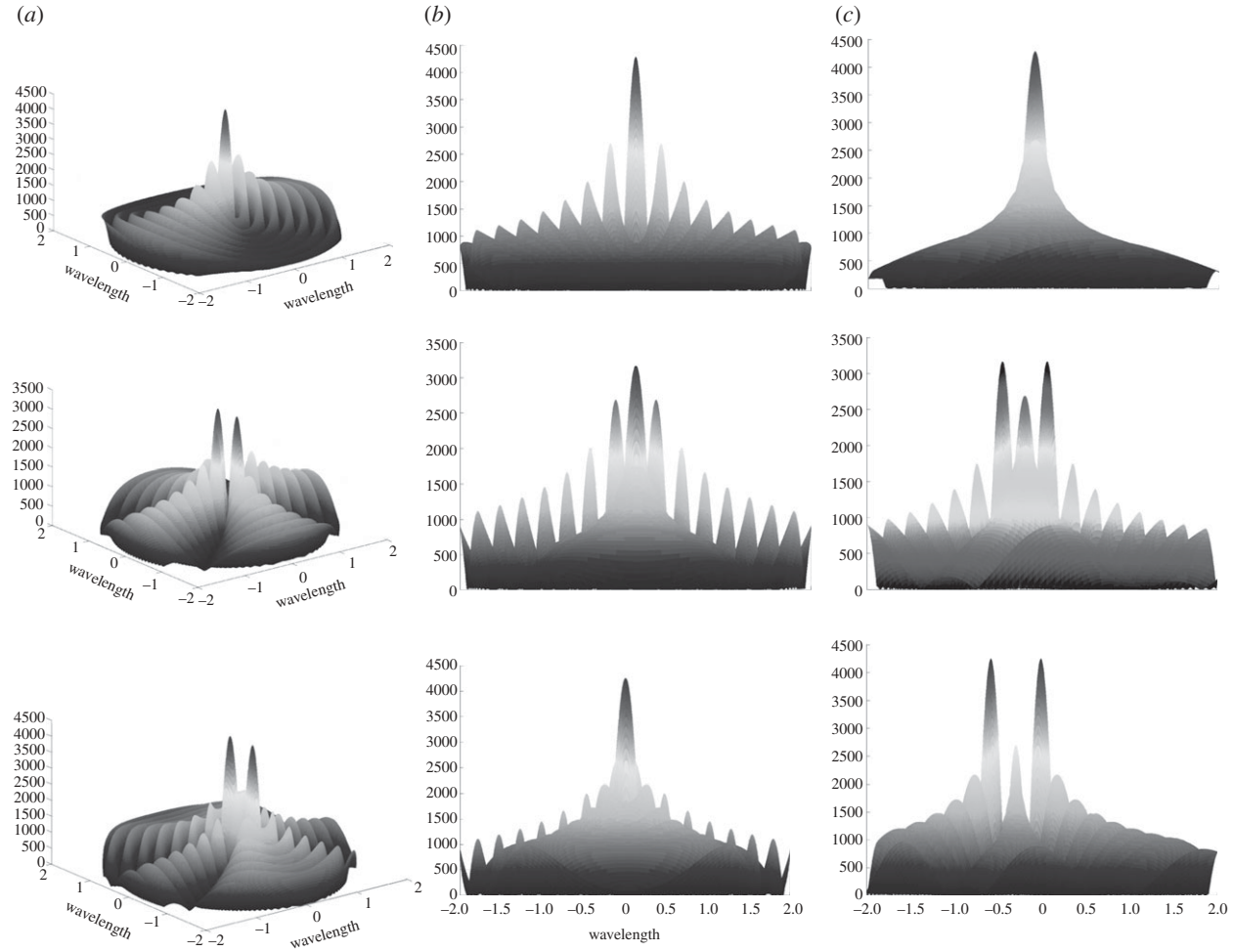

Figure 4. Simulated coherent Doppler tomographic images of two scatterers with various separations. (*a*) XYZ view, (*b*) XZ view, and (*c*) YZ view.

about 0.24λ, implying that two points can be seen separated from each other if they are 0.24λ away from each other. However, if the side-lobe amplitudes are too high, they will not be separable. Figure 4 shows an example in which one scatterer is simulated at the centre of rotation (i.e. at $r_1 = 0$) and a second scatterer is simulated at $r_2 = 0.2\lambda$, 0.38λ and 0.6λ away from the first scatterer. A target can be detected in the centre of rotation even there is no Doppler shift there. If we receive reflection from a transmission and there is no Doppler shift, there must be a target in the centre of rotation. The plots show that, at 0.2λ, the scatterers are combined. From 0.38λ onwards, the two scatterers are separated with main lobes stronger than those of the first side lobes. The reason for the high resolution achieved with coherent DT is that coherently processing (summing) the data acquired through the whole revolution can be regarded as synthesizing a physical aperture

which is circular. In US and microwave imaging, the larger the aperture, the better the spatial resolution.

2.3.2. Image reconstruction

2.3.2.1. Cartesian coordinates. As described earlier (and see equation (2.5)), the reconstruction of the coherent DT image is based on the two-dimensional Fourier transform, which maps points in data space on a Cartesian raster to points in the frequency domain and also on a Cartesian raster. However, the measured points are on a polar raster (i.e. $S(\boldsymbol{\Theta})$) and, therefore, they are not compatible with the required input to the digital algorithm for two-dimensional Fourier transformation. Consequently, the question is how to make $S(\boldsymbol{\Theta}) \rightarrow S(f_x, f_y)$. One possible solution is to interpolate from the one-dimensional measured points in the polar raster to the sample needed for the two-dimensional Cartesian raster. A two-dimensional Fourier transform is then performed to get an estimate of the object reflectivity on a rectangular raster. With this approach, the quality of the final image is very dependent upon the method of two-dimensional interpolation: the higher the order of the interpolation, the better the image quality. However, using high-order interpolation significantly adds to the computational complexity and to the total time required for reconstructing the image.

2.3.2.2. Polar coordinates. Alternatively, interpolation can be bypassed and the potential error owing to interpolation is avoided if the required inverse Fourier transformation is performed on a polar raster [20]. The predicted image becomes

$$\hat{g}(r,\theta) = \frac{2}{\lambda}\int_0^{2\pi} S(\boldsymbol{\Theta}) \exp\left[-j\frac{4\pi}{\lambda} r\cos(\theta - \boldsymbol{\Theta})\right] \mathrm{d}\boldsymbol{\Theta}, \quad (2.7)$$

where $S(\boldsymbol{\Theta})$ is the observed data. It can be seen that equation (2.7) is a periodic convolution, which can be computed using a fast convolution algorithm. The tomographic image is reconstructed by repeating the periodic convolution for each radius increment Δr.

2.3.3. Experimental results. Experiments were conducted using a prototype two-dimensional DT scanner with a small rotating object (phantom) insonated by CW US in water [23]. A 9.79 MHz US probe (made in our laboratory in the 1970s) was positioned just under the water surface, 150 mm away from and directly facing the phantom. The probe was driven by a Doppler instrument [4], which also amplified and demodulated the returned signals. The I/Q signals were sampled by the sound card of a PC (16-bit resolution, 44.1 kHz sampling rate, two channels). The phantom was rotated at a preselected constant angular speed, so that the samples that were obtained from the sound card were the angular samples needed for coherent DT.

Various phantoms were used to test the coherent DT system. The first was a single needle phantom. The needle was 0.5 mm in diameter and 40 mm long. About 35 mm of the needle was immersed into the water. The needle was 5 mm away from the centre of rotation and the distance between the probe and the phantom was about 150 mm. The experiment was conducted such that data were recorded with rotation speeds ranging from 0.5 to 25 rotations per second (r.p.s.). The maximum Doppler frequency at 25 r.p.s. was less than 11 kHz, so the 44.1 kHz sampling rate was sufficient.

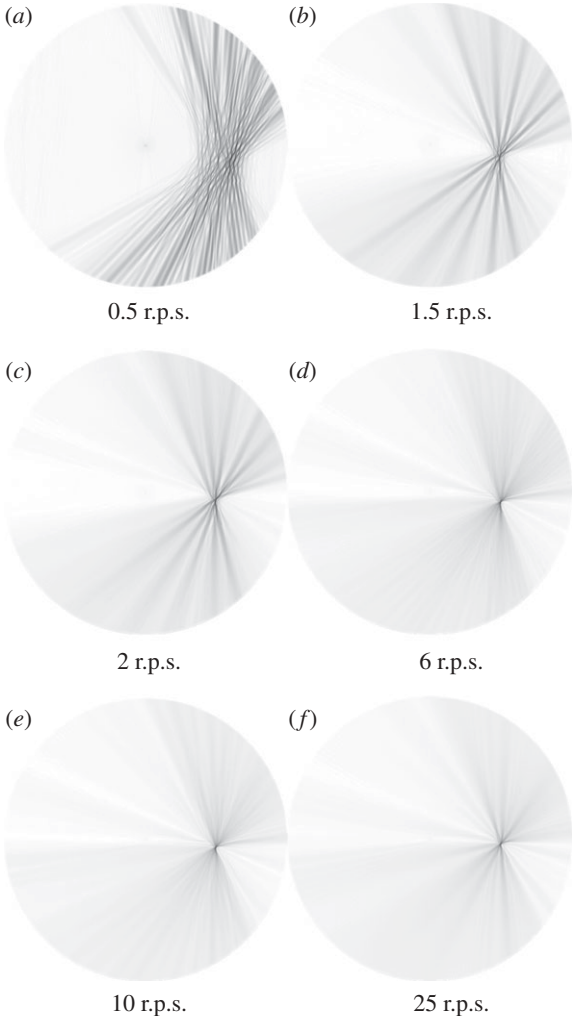

Figure 5. Ten megahertz coherent Doppler tomographic images of a single stainless-steel needle at various rotation speeds.

Figure 5 is a selection of reconstructed coherent DT images. The images with slow speeds of rotation (i.e. from 0.5 r.p.s.) are more fuzzy near the target area and are thus unable to provide a good indication of target position because, when the phantom was rotated at slow speed, it could not generate a sufficient dynamic range of Doppler shift frequencies for detection, owing to the frequency response of the equipment. However, better results were achieved when the rotation speed was increased to 2 r.p.s. and beyond. Figure 6 shows the corresponding images, before and after thresholding at 50 per cent maximum.

The second phantom consisted of eight 0.05 mm diameter copper wires; four copper wires were about 13 mm away from the centre of rotation and the other four were about 7 mm away from the centre of rotation. All the copper wires and the axis of rotation were orthogonal to the water surface. Figure 7 shows the coherent DT image of the wire phantom rotated at

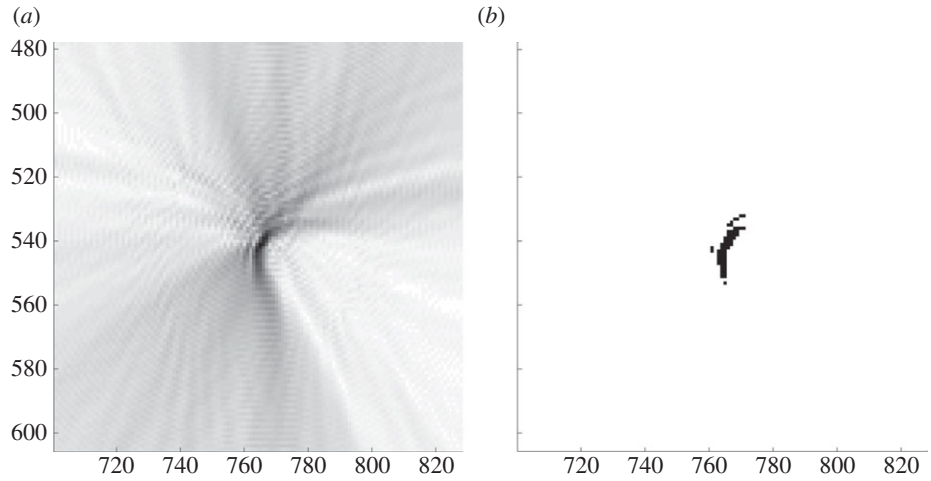

Figure 6. Zoomed-in 10 MHz coherent Doppler tomographic images of a needle at 10 r.p.s. (*a*) Original image and (*b*) image thresholded with 50% maximum.

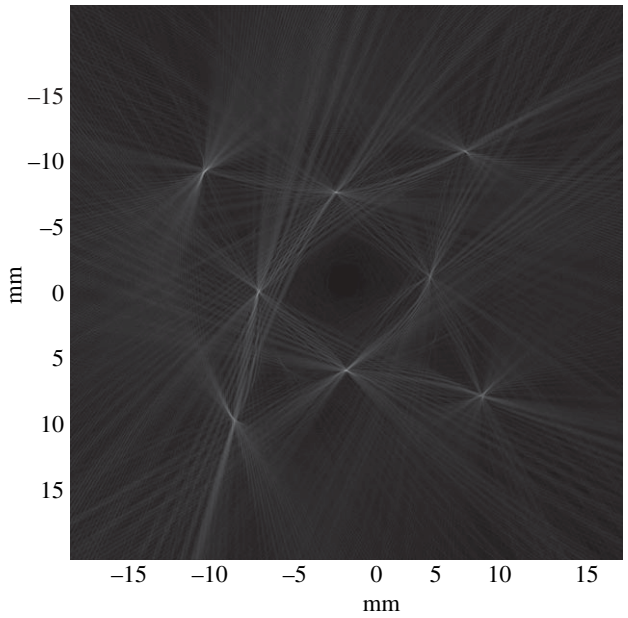

Figure 7. Image of eight copper wires rotated at 2 r.p.s.

2 r.p.s. It can be seen that the distances between the wires and the dimensions of the reconstructed image were virtually the same as those of the actual phantom.

3. LINEAR DOPPLER TOMOGRAPHY

An alternative approach to either rotating the object or rotating the probe around the object to cause the Doppler effect for imaging is to translate the probe in a linear motion to get a similar effect [8]. An US transducer is moved along a straight line with constant velocity (v), sending out a single frequency (f_0) sinusoidal plane wave tone burst encompassing the whole object (figure 8). The received US signal will have frequency shift corresponding to the direction angle. The amplitude of a given frequency shift is the sum of all the reflected waves from along the line at the corresponding angle. The frequency spectrum can be

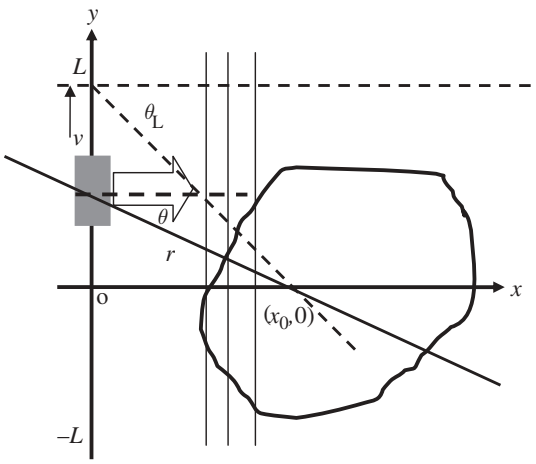

Figure 8. Geometry of linear Doppler tomography. The US beam points towards right, encompassing the whole object. L is the end of travel of the transducer.

interpreted as the projection of the reflectivity along the line at that angle. At another transducer position with different direction angle, another projection can be obtained, and so on. An image of the targets can then be reconstructed by backprojection.

Just as with the incoherent processing method described in the circular motion mode, the period of time used to receive the signal is important. If it is too short, the frequency spectrum cannot be determined precisely. If it is too long, the transducer will travel a long distance, thus changing the scattering angle. The optimum length for the period of receiving the signal has been shown [8] to be

$$T_{\mathrm{p}} = \frac{1}{v\cos\theta_{\mathrm{t}}}\left(\frac{cr_{\mathrm{t}}}{2f_0}\right)^{1/2} = \frac{1}{v\cos\theta_{\mathrm{t}}}\left(\frac{\lambda r_{\mathrm{t}}}{2}\right)^{1/2}, \qquad (3.1)$$

where c is the speed of sound and θ_{t} and r_{t} are the direction angle and the distance between the transducer and the object, respectively.

The x and y directions of the imaging resolution depend on the velocity and position of the transducer and

scattering angle. If the data are processed incoherently (amplitude only),

$$\Delta y_{\mathrm{r}} = \frac{cx_0}{2f_0 v T_{\mathrm{p}}} = \frac{\lambda x_0}{2v T_{\mathrm{p}}} \tag{3.2}$$

and

$$\Delta x_{\mathrm{r}} = \frac{\Delta y_{\mathrm{r}}}{\sin\theta_{\mathrm{L}}}. \tag{3.3}$$

The definition of θ_{L} can be found in figure 8. If both the amplitude and the phase are retained and backprojection is applied coherently, the resolution is

$$\Delta y_{\mathrm{r}} = \frac{c}{2f_0 \tan\theta_{\mathrm{L}}} \tag{3.4}$$

and the resolution in the x direction is the same as that in the y direction. Using reported parameters [8] ($c = 1500\ \mathrm{m\,s^{-1}}$, $f_0 = 3.3$ MHz, $x_0 = 64$ mm, $\theta_{\mathrm{L}} = 45^{\circ}$) in the incoherent case, $\Delta y_{\mathrm{r}} = \Delta x_{\mathrm{r}} = 2.7$ mm, and, in the coherent case, $\Delta y_{\mathrm{r}} = 0.2$ mm, which is around 0.45 wavelength. The high resolution of coherent imaging is due to the synthesis of a large aperture by coherently processing the data from various locations. The reported experimental results confirmed the high resolution of the coherent imaging method, but with apparent high side lobes [8]. In that experiment, the US frequency was 3.4 MHz, the period of the sinusoidal tone burst signal was 58 ms and the transducer movement speed was $110\ \mathrm{mm\,s^{-1}}$. As the duration of the tone burst was so long compared with that of the period of the US, the signal can be regarded as CW.

4. DISCUSSION AND CONCLUSIONS

DT uses CW US and, as a result, it is a narrow-bandwidth and high-sensitivity technique because the ultrasonic and electrical signals are confined to a very small range of frequencies. This permits the use of low-noise electronics and transducers that have a low insertion loss, i.e. little energy is lost during the conversion from electrical signal to mechanical vibration and vice versa. The effective penetration is also deeper than conventional pulse-echo B-scan owing to the high efficiency of the CW probe.

Although continuous emission greatly simplifies the design and construction of the electronic system, it prevents the emitting piezoelectric transducer from also being used to detect the scattered US waves, because the dynamic range is too great. Therefore, a separate piezoelectric transducer is needed for reception and this is usually incorporated into the same probe. The transmitter and receiver should point to the same direction. However, in practice, they are at a small angle and only part of the US beam is coincident. This should be taken into account during image reconstruction.

It has been proposed [24] to replace the FT-based frequency spectrum analysis with (Morlet) wavelet-based frequency analysis in microwave Doppler imaging. The recorded one-dimensional signal is wavelet-transformed to obtain the temporal frequency variation at different aspect angles. Then, a two-dimensional image can be reconstructed by backprojecting (integrating) the aspect-Doppler diagram.

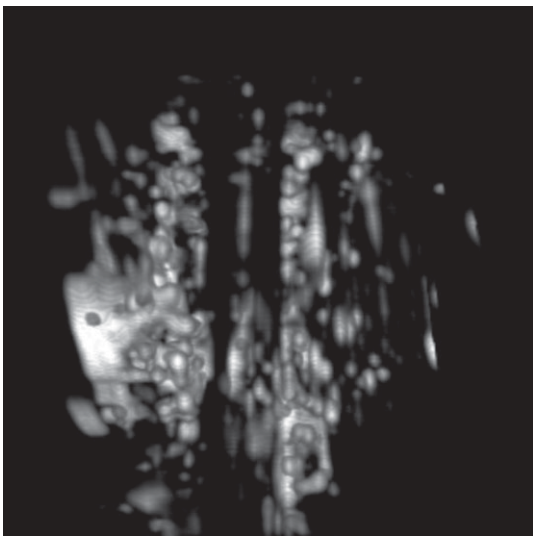

Figure 9. Three-dimensional image of a bovine coccygeal intervertebral disc based on incoherent Doppler tomography.

In the circular DT, as some time is required for the probe to rotate around tissue, there will be some movements by the patient even when breath-holding. The centre of rotation could also change owing to the movements. Motion compensation should be investigated when this technology is to be developed clinically. Image blurring and clarity will strongly depend on the accuracy of motion compensation.

In practical patient scanning, the targets will probably need to be in the near field of the US beam, where the beam profile is non-uniform, and this will degrade the image. This degradation will probably need to be ameliorated, for example by beam profile compensation, aperture apodization and beam-sweeping. For biological sites with bone or gas, there will be strong reflections and the targets beyond the bone or gas will contribute less to the spectra of Doppler shift. However, these targets will contribute more when the US probe rotates to other positions where the US beams are not blocked by bone or gas. It could still be possible to obtain reasonable images. This resembles compound US scanning, where bone or gas pose a lesser problem than in conventional B-mode scanning.

DT is different from conventional UCT in that DT uses CW while UCT uses pulsed US. There are two types of UCT: transmission [25] and reflection [26]. The former is used to determine the attenuation and speed of sound in tissues. The latter is used to detect the reflectivity of targets. DT only detects reflectivity. It also needs relative motion between probe and tissue while UCT does not.

The development of DT is still in its early stages. There has been little application of DT in biological tissues apart from the work done by Liang *et al.* [12]. A three-dimensional image of bovine coccygeal intervertebral discs was reconstructed from 34 separate two-dimensional slices acquired from different positions along the rotation axis (figure 9). The annular structure of the disc can be clearly seen. The vertebra can also be seen.

In medical imaging, three-dimensional images can provide extra information that cannot be revealed by

two-dimensional images. Often, three-dimensional images are formed by stacking parallel two-dimensional images in a volumetric dataset. Three-dimensional DT images can be created by translating the probe along the direction of the axis of rotation [12]. An alternative is first to rotate the probe around the rotation axis of the target and then to move the probe in a plane containing the rotation axis of the target but at an angle to it. The probe mounting will need to be designed to allow up to 90° adjustment relative to the rotation axis, so that the US beam can look at the targets at various (insonation) angles. Thus, the backscattered fields will be acquired as a function of three parameters: CW frequency, azimuth position of the rotating platform and insonation angle. Three-dimensional reconstruction will then be possible [27,28].

Much work remains to be done before DT will be developed to a stage suitable for clinical evaluation. This includes motion compensation, near-field US beam formation, side-lobe suppression, speckle reduction and attenuation compensation. It is already apparent that the technique has the potential to achieve a spatial resolution substantially better than that which can be obtained with traditional pulse-echo imaging at the same ultrasonic frequency. The potential applications could include breast imaging for cancer detection.

This work was supported by grants from the UK Engineering and Physical Sciences Research Council (GR/M07861) and the National Institute for Health Research (NIHR) Invention for Innovation (i4i) programme (II-FS-0109-11071). This report presents independent research commissioned by the NIHR. The views expressed are those or the authors and not necessarily those of the NHS, the NIHR or the Department of Health.

REFERENCES

1 Wells, P. N. T. 2000 Current status and future technical advances of ultrasonic imaging. *IEEE Eng. Med. Biol. Mag.* **19**, 14–20. (doi:10.1109/51.870227)
2 Taylor, K. J. W., Burns, P. N. & Wells, P. N. T. 1988 *Clinical applications of Doppler ultrasound*. New York, NY: Raven Press.
3 Wells, P. N. T. & Skidmore, R. 1985 Doppler developments in the last quinquennium. *Ultrasound Med. Biol.* **11**, 613–623. (doi:10.1016/0301-5629(85)90034-1)
4 Liang, H. D., Halliwell, M. & Wells, P. N. T. 2001 Continuous wave ultrasonic tomography. *IEEE Trans. Ultrason. Ferroelectr. Freq. Control* **48**, 285–292. (doi:10.1109/58.896141)
5 Greenleaf, J. F. & Bahn, R. C. 1982 Breast scanning with ultrasonic computer-assisted tomography. *Ultrasound Med. Biol.* **8**, 453.
6 Greenleaf, J. F., Gisvold, J. J. & Bahn, R. C. 1982 Computed transmission ultrasound tomography. *Med. Prog. Technol.* **9**, 165–170.
7 Greenleaf, J. F. & Ylitalo, J. 1986 Doppler tomography. In *Proc. IEEE Ultrasonic Symp., Williamsburg, VA, 1719 November 1986*, pp. 837–841.
8 Nagai, K. & Greenleaf, J. F. 1990 Ultrasonic-imaging using the Doppler-effect caused by a moving transducer. *Opt. Eng.* **29**, 1249–1254. (doi:10.1117/12.55709)
9 Wade, G., Elliott, S., Khogeer, I., Flesher, G., Eisler, J., Mensa, D. N., Ramesh, S. & Heidbreder, G. 1978 Acoustic echo computer tomography. In *Acoustical imaging*, vol. 8 (ed. A. F. Metherell), pp. 565–576. New York, NY: Plenum Press.
10 Liang, H. D., Halliwell, M. & Wells, P. N. T. 2000 Doppler ultrasonic imaging. In *Acoustical imaging*, vol. 25 (eds M. Halliwell & P. N. T. Wells), pp. 279–288. New York, NY: Plenum Press.
11 Liang, H. D., Halliwell, M. & Wells, P. N. T. 2001 Continuous wave ultrasonic tomography in NDE. *Prog. Nat. Sci.* **11**, S151–S155.
12 Liang, H. D., Halliwell, M., Johnson, S. & Wells, P. N. T. 2003 Incoherent imaging using continuous wave ultrasound. A preliminary study using bovine intervertebral disc. *Eur. J. Ultrasound* **16**, 253–260. (doi:10.1016/S0929-8266(02)00080-0)
13 Hagfors, T. & Campbell, D. B. 1973 Mapping of planetary surfaces by radar. *Proc. IEEE* **61**, 1219–1225. (doi:10.1109/PROC.1973.9248)
14 Walker, J. L. 1980 Range-Doppler imaging of rotating objects. *IEEE Trans. Aerosp. Electron. Syst.* **16**, 23–52. (doi:10.1109/TAES.1980.308875)
15 Brown, W. M. & Fredrick, R. J. 1969 Range-Doppler imaging with motion through resolution cells. *IEEE Trans. Aerosp. Electron. Syst.* **5**, 98–102. (doi:10.1109/TAES.1969.309826)
16 Chen, C. C. & Andrews, H. C. 1980 Multifrequency imaging of radar turntable data. *IEEE Trans. Aerosp. Electron. Syst.* **16**, 15–22. (doi:10.1109/TAES.1980.308874)
17 Chen, C. C. & Andrews, H. C. 1980 Target-motion-induced radar imaging. *IEEE Trans. Aerosp. Electron. Syst.* **16**, 2–14. (doi:10.1109/TAES.1980.308873)
18 Kalender, W. A. 2006 X-ray computed tomography. *Phys. Med. Biol.* **51**, R29–R43. (doi:10.1088/0031-9155/51/13/R03)
19 Mensa, D. L., Heidbreder, G. R. & Wade, G. 1980 Aperture synthesis by object rotation in coherent imaging. *IEEE Trans. Nucl. Sci.* **27**, 989–998. (doi:10.1109/TNS.1980.4330965)
20 Mensa, D. L., Halevy, S. & Wade, G. 1983 Coherent Doppler tomography for microwave imaging. *Proc. IEEE.* **71**, 254–261. (doi:10.1109/PROC.1983.12563)
21 Berizzi, F. & Corsini, G. 1999 A new fast method for the reconstruction of 2-D microwave images of rotating objects. *IEEE Trans. Image Process.* **8**, 679–687. (doi:10.1109/83.760335)
22 Mensa, D. L. & Heidbreder, G. 1982 Bistatic synthetic-aperture radar imaging of rotating objects. *IEEE Trans. Aerosp. Electron. Syst.* **18**, 423–431. (doi:10.1109/TAES.1982.309249)
23 Tsui, C. S. L., Liang, H. D., Halliwell, M., Shere, M., Braybrooke, J. P., Whipp, E. & Wells, P. N. T. 2011 Coherent ultrasonic Doppler tomography. *Ultrasound Med. Biol.* **37**, 642–650.
24 Su, C. N., Fu, I. J. & Chang, D. C. 1995 New approach to Doppler tomography for microwave imaging. *Int. J. Electron.* **78**, 209–218. (doi:10.1080/00207219508926152)
25 Greenleaf, J. F. 1983 Computerized-tomography with ultrasound. *Proc. IEEE* **71**, 330–337. (doi:10.1109/PROC.1983.12591)
26 Dines, K. A. & Goss, S. A. 1987 Computed ultrasonic reflection tomography. *IEEE Trans. Ultrason. Ferroelectr. Freq. Control* **34**, 309–318. (doi:10.1109/T-UFFC.1987.26949)
27 Knaell, K. K. & Cardillo, G. P. 1995 Radar tomography for the generation of 3-dimensional images. *IEE Proc. Radar Sonar Navig.* **142**, 54–60. (doi:10.1049/ip-rsn:19951791)
28 Fortuny, J. & Sieber, A. J. 1999 Three-dimensional synthetic aperture radar imaging of a fir tree: first results. *IEEE Trans. Geosci. Rem. Sens.* **37**, 1006–1014. (doi:10.1109/36.752219)